

In Situ Measurement of Instantaneous Viscosity Curve of Fluids in a Reserve Tank

Taiki Yoshida,* Kohei Ohie, and Yuji Tasaka



Cite This: *Ind. Eng. Chem. Res.* 2022, 61, 11579–11588



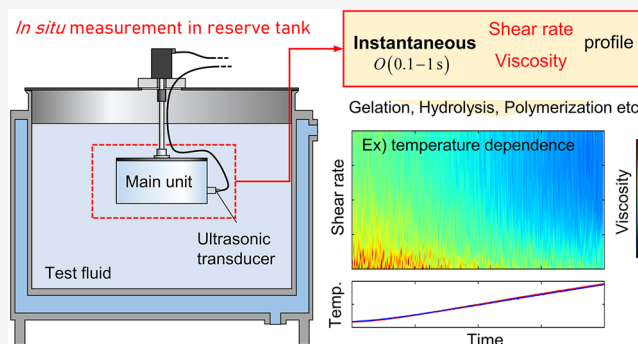
Read Online

ACCESS |

Metrics & More

Article Recommendations

ABSTRACT: A novel method enabling *in situ* measurement in a reserve tank for evaluating an instantaneous viscosity curve is presented. This aims to satisfy the practical demand of industrial production process for monitoring real-time rheological properties without taking samples. With applicable ranges of shear rate and viscosity, $O(10^{-1}-10^2 \text{ s}^{-1})$ and $O(10^{-2}-10^0 \text{ Pa}\cdot\text{s})$, it enables evaluation of fluid properties having shear strain rate dependence, based on ultrasonic spinning rheometry. Since this method evaluates the characteristic of shear thinning viscosity while changing the fluid temperature in a reserve tank, some useful examples are expected as further applications for measuring viscosity during chemical reaction processes, such as gelation, hydrolysis, and polymerization. Efficacy of the method evaluating rheological properties is validated by numerical and experimental results.



1. INTRODUCTION

In the production processes of various materials, such as food, polymer, and resin, the control and measurement of product quality are crucial not only for optimizing the process but also for improving product quality. Evaluating rheological properties is most important for assessing the production quality, so various rheometers have progressively been enhanced and commercially supplied as a key tool for evaluating properties. One of the representative principles in a rheometer is a measurement type sensing axial torque via solid walls with a specific gap and having various geometries (parallel-disk, plate/cone disk, coaxial double cylinder, and more). To ensure measurement accuracy, stable and ideal conditions are required for the use of these rheometers; thus, taking a sample is needed for evaluating the rheological properties. Considering the actual requirements in industrial production sites, rheometers that require some amount of sample do not fully satisfy the industrial demands because most fluid products are hermetically sealed, preserved in a reserve tank, or flowed in pipelines. To satisfy the demands, *in situ* measurement for evaluating rheological properties is of considerable interest.

Some studies on the development of an *in situ* measurement method for evaluating rheological properties are as follows. Broadhead et al. developed an in-line rheometer, which utilizes the principle of a Couette flow viscometer.¹ Covas et al. conducted an experiment where a standard torque rheometer is inserted at different locations along an extruder for monitoring variations of polymer characteristics.² Glasscock et al. inserted a rheometer with parallel-plate geometry into the

pipeline.³ All these developments divert a standard rheometer as an in-line or on-line measurement system for monitoring rheological properties. Because ideal conditions are absolutely imperative for standard torque rheometers in order to ensure accuracy, *in situ* measurement based on sensing torque force is impractical in cases measuring complex fluid conditions, such as multiphase. The difficulties in using standard torque rheometers for evaluating non-Newtonian fluids are reported in many previous researches, for example, refs 4–6.

Other developments of an *in situ* measurement method based on unique principles are introduced below. Guillemain et al. developed a mixer-type rheometer consisting of a mixing device with a quite complex geometry that rotates in a cylindrical tank.⁷ Coogan and Kazmer developed a novel in-line method, termed a fused deposition modeling rheometer (FDMRheo).⁸ This enables rheological property evaluation as a function of a fused deposition modeling printer. Wallevik et al. numerically analyzed the relationship between the power required to turn the drum of a concrete mixing truck and the rheological properties of the fresh concrete.⁹ Due to the complexity of fluid properties and its behaviors, the rheological

Received: May 21, 2022

Revised: July 19, 2022

Accepted: July 20, 2022

Published: July 30, 2022



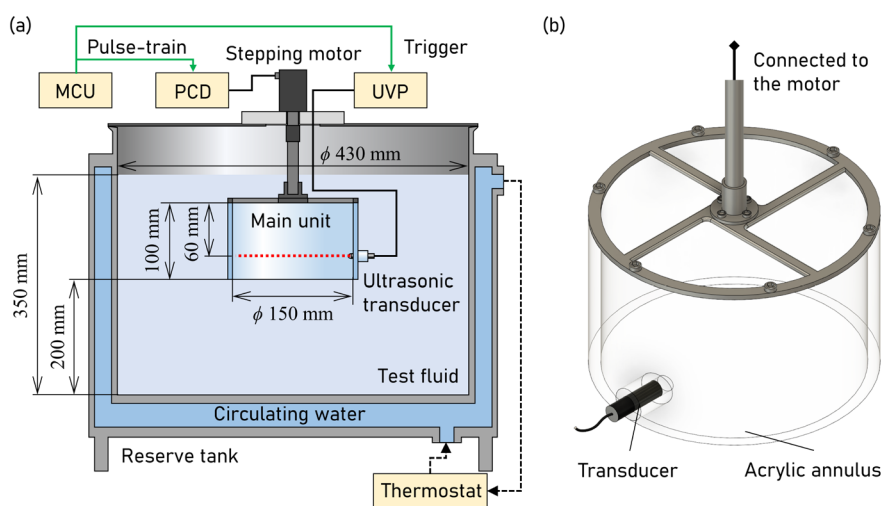


Figure 1. (a) Schematic of experimental apparatus. (b) Enlarged view of main unit.

evaluations of these methodologies are based on the empirical relation of a mechanical response arising from various experimental geometries, so the scope of target are limited. Thus, when a fluid with unknown properties is measured, the obtained data is no more than a correct value as a relative evaluation.

For satisfying industrial demands, measuring fluid motion is key because all rheological information is reflected in it, as long as the fluid flow obeys the equation of motion. Some researches have focused on development of rheometries coupled with spatiotemporal velocity-profiling techniques. This is termed velocity-profiling rheometry; for example, Dimitriou et al. developed a Rheo-PIV system which utilizes particle imaging velocimetry (PIV) in order to obtain the actual shear rate in the narrow gap of standard rheometer.¹⁰ Martin and Hu utilized particle tracking velocimetry in order to obtain the actual shear rate in the narrow gap of a standard rheometer for elucidating transient and steady-state shear banding.¹¹ Derakhshandeh et al. utilized ultrasonic velocity profiling (UVP), combining it with a standard rotational rheometer for evaluating fluids having thixotropic characteristics.¹² Gallot et al. developed an ultrasonic imaging technique that enables measurement of unstable shear-banded flow of a non-Newtonian fluid.¹³ In these developments, the velocity-profiling rheometries give solutions to clarify many issues on measurement techniques in rheology, such as shear banding,^{14,15} elastic instability,^{16,17} wall-slip,⁵ and more. As examples of in-line rheometry utilizing velocity profiling, Wiklund et al. developed UVP-PD in-line rheometry, which is a UVP technique combined with pressure difference (PD) measurements.¹⁸ Most recently, Tasaka et al. presented a nonintrusive in-line rheometry using UVP without a pressure drop measurement.¹⁹ Thus, in multiple studies, velocity-profiling rheometry has been intensively developed and shown successful results for evaluating rheological properties of fluid with complex characteristics.

To satisfy the industrial demands mentioned above and to establish a novel rheometer based on velocity profiling, the present study aims to develop a novel *in situ* measurement tool for evaluating rheological properties of fluids in a reserve tank without taking a fluid sample. The fundamental principle of this tool is ultrasonic spinning rheometry (USR),^{20–28} which was developed based on the theory of fluid mechanics. In this

USR, velocity data in fluid flow is substituted into the equation of motion to solve it. The measurement setup is an open cylindrical container mounted at the center of a large water bath having a size of $1000 \times 1000 \text{ mm}^2$. This bath size is required to measure velocity to minimize the influence as much as possible from co-reflected ultrasonic waves according to previous developments.²¹ Although the efficacy of USR has been ensured by comparative experiments with a standard rheometer and applications to various complex fluids in previous studies mentioned above, the experimental configuration limits the USR evaluations as a method taking some amount of sample, which is the same condition as standard torque rheometers. To solve this limitation, in this study, an ultrasonic transducer for measuring velocity profile is embedded in the oscillating annulus generating unsteady flow. This union allows crucial functions as an *in situ* measurement tool for evaluating fluid properties in a reserve tank: (1) instantaneous measurement of shear rate profile, (2) *in situ* measurement in reserve tank without taking samples, and (3) evaluation of rheological properties with transient change. To visualize fluid properties in the tank, there is a possibility of further application, such as viscosity changes in the process of chemical reactions, such as gelation, hydrolysis, and polymerization. In this study, the efficacy of the evaluation method is ensured through numerical validation and experiments.

2. BASIC CONCEPT AND RHEOMETER DESIGN

The entire schematic of experimental apparatus is shown in Figure 1a. The main unit for evaluating rheological properties, an annulus made of acrylic resin, is hung from the lid of a reserve tank. The tank has a 430 mm inner diameter and is made of stainless steel with a jacket for controlling the temperature of the test fluid by thermostat. The fluid temperature evaluating the rheological properties is determined as $T = (T_{\text{top}} + T_{\text{bottom}})/2$, where T_{top} and T_{bottom} are the temperatures measured at the top and bottom of tank, and the temperature difference $|T_{\text{top}} - T_{\text{bottom}}|$ is no more than $1 \text{ }^\circ\text{C}$. The bottom of main unit was placed so that there is a 200 mm distance from the bottom of tank. The height of test fluid level was around 350 mm. A stepping motor fixed on the lid oscillates the main unit so that the annulus wall takes a sinusoidal velocity, $U_{\text{wall}} \sin 2\pi f_0 t$, where $U_{\text{wall}} = 2\pi f_0 R\Theta$. Here

Θ and f_0 denote the oscillation amplitude and frequency. A microcontroller unit (MCU) generates a pulse train for controlling the stepping motor and the trigger pulse for synchronizing the oscillation start with the measurement start of UVP. Arduino Mega 2560 is used as the MCU, which is available as an open-source electronics platform. The transmitted pulse train signals are encoded by a pulse-control driver (PCD; CVD528B-K, Oriental Motor, Corp.) for the controlling the stepping motor (PKP566N28A2, Oriental Motor, Corp.).

An enlarged view of main unit is shown in Figure 1b, including the acrylic annulus having a 10 mm thick wall, a 150 mm inner diameter, and a 100 mm height. The annulus is supported by stainless frame with the shape shown in Figure 1b. Here, the frame was designed to suppress the occurrence of secondary flow in the annulus, which prevents accurate evaluation of rheological properties. The influence of such flow prevention has been reported by Ohie et al.²⁹

A schematic of vector arrangement in the cross section of main unit is drawn in Figure 2. To measure instantaneous

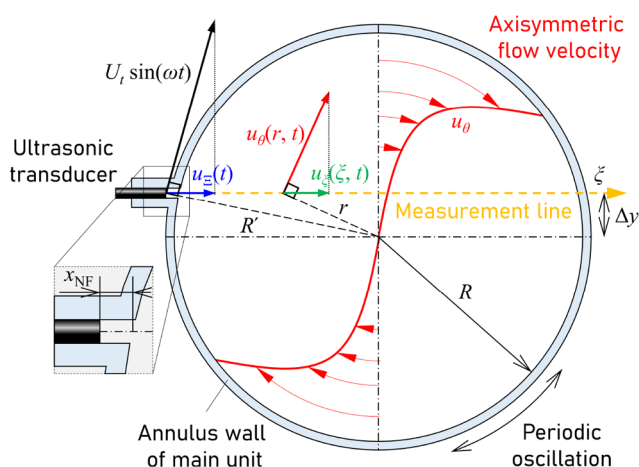


Figure 2. Schematic of vector arrangements on the measurement line of ultrasound velocity profiling.

velocity profiles, the UVP-Model Duo (Met-Flow S.A., Switzerland) was used. An ultrasonic transducer was embedded in the lateral side of main unit, which has a 4 MHz resonance frequency and 5 mm active element diameter. By analyzing the Doppler frequency in the ultrasonic echo, the flow velocity can be evaluated at equal intervals on the transducer measuring axis. In the UVP method, unidirectional velocity component perpendicular to pulse emission surface in ultrasonic transducer can be measured. The time, spatial, and velocity resolutions are $O(10 \text{ ms})$, $O(0.1 \text{ mm})$, and $O(0.1 \text{ mm/s})$, respectively. Here, for obtaining the azimuthal velocity component u_θ , the transducer was placed with a gap $\Delta y = 18 \text{ mm}$ from the central axis of the annulus. Because the transducer oscillates accompanied by the motion of annulus, the measured velocity u_m is represented as

$$u_m = u_\xi + u_\Xi \quad (1)$$

where u_ξ and u_Ξ indicate the components of fluid flow velocity and transducer motion along the direction of ultrasonic beam path. Thus, the relative velocity should be considered to obtain the azimuthal velocity from u_m .

Assuming that the flow field in the annulus is assumed to be axisymmetric with radial component of negligible small velocity, u_ξ is calculated as

$$u_\xi = u_\theta \frac{\Delta y}{r} \quad (2)$$

where

$$r = \sqrt{\Delta y^2 + (\sqrt{R^2 - \Delta y^2} - \xi)^2} \quad (3)$$

The origin of ξ is defined at the inner surface of annulus. In addition, the azimuthal velocity of the transducer embedded in the annulus wall is measured as

$$u_\Xi = U_t \sin(\omega t) \frac{\Delta y}{R'} \quad (4)$$

where $U_t = 2\pi f_0 R' \Theta$. R' represents the radial position of the transducer surface

$$R' = \sqrt{R^2 + x_{\text{NF}}^2 + 2x_{\text{NF}}\sqrt{R^2 - \Delta y^2}} \quad (5)$$

x_{NF} indicates the gap between front face of the transducer and the inner surface of the annulus as shown in Figure 2. This gap is important to avoid overlapping the measurement region with the “near-field” of the ultrasonic beam, which is an unmeasurable region because of the transient state of the ultrasound pulse beam. Measuring the velocity by the transducer that moves with the annulus is different from velocity measurement under conventional USR conditions in Yoshida et al.²⁴ The transducer arrangement in conventional USR was independent from the oscillation of cylindrical container. In contrast, because the transducer moves accompanied by the annulus oscillation, the measured velocity u_m gets smaller as the radial position becomes closer to the annulus wall. Thus, the influence of the S/N ratio in the measured velocity is also different comparing the present method with the conventional USR. This design confers a practical benefit where the ultrasonic waves easily propagate into fluid media because of direct contact of the transducer to the test fluid. The advantage due to the embedded transducer on the evaluation is explained below. In section 3.1, we investigated numerically whether the moving transducer affects the accuracy in evaluations of rheological properties.

For evaluating the rheological properties, the velocity data is substituted into formulas of Cauchy’s equation of motion and constitutive equation

$$\rho \frac{\partial u_\theta}{\partial t} = \frac{\partial \tau}{\partial r} + \frac{2\tau}{r} \quad (6)$$

$$\tau + \frac{1}{\omega_0 \tan \delta} \frac{\partial \tau}{\partial t} = \mu \dot{\gamma} \quad (7)$$

where τ , $\dot{\gamma}$, and ω_0 denote shear stress, shear strain rate, and angular frequency of annulus oscillation, respectively. Here, $\dot{\gamma}$ can be obtained by

$$\dot{\gamma} = \frac{\partial u_\theta}{\partial r} - \frac{u_\theta}{r} \quad (8)$$

where $\dot{\gamma}$ is defined as an effective value calculating root-mean-square, since it fluctuates with a periodic sine wave. The formula of eq 6 is simplified, assuming that the flow field inside the annulus is axisymmetric with a radial component of negligibly small velocity. Here it should be noted that the

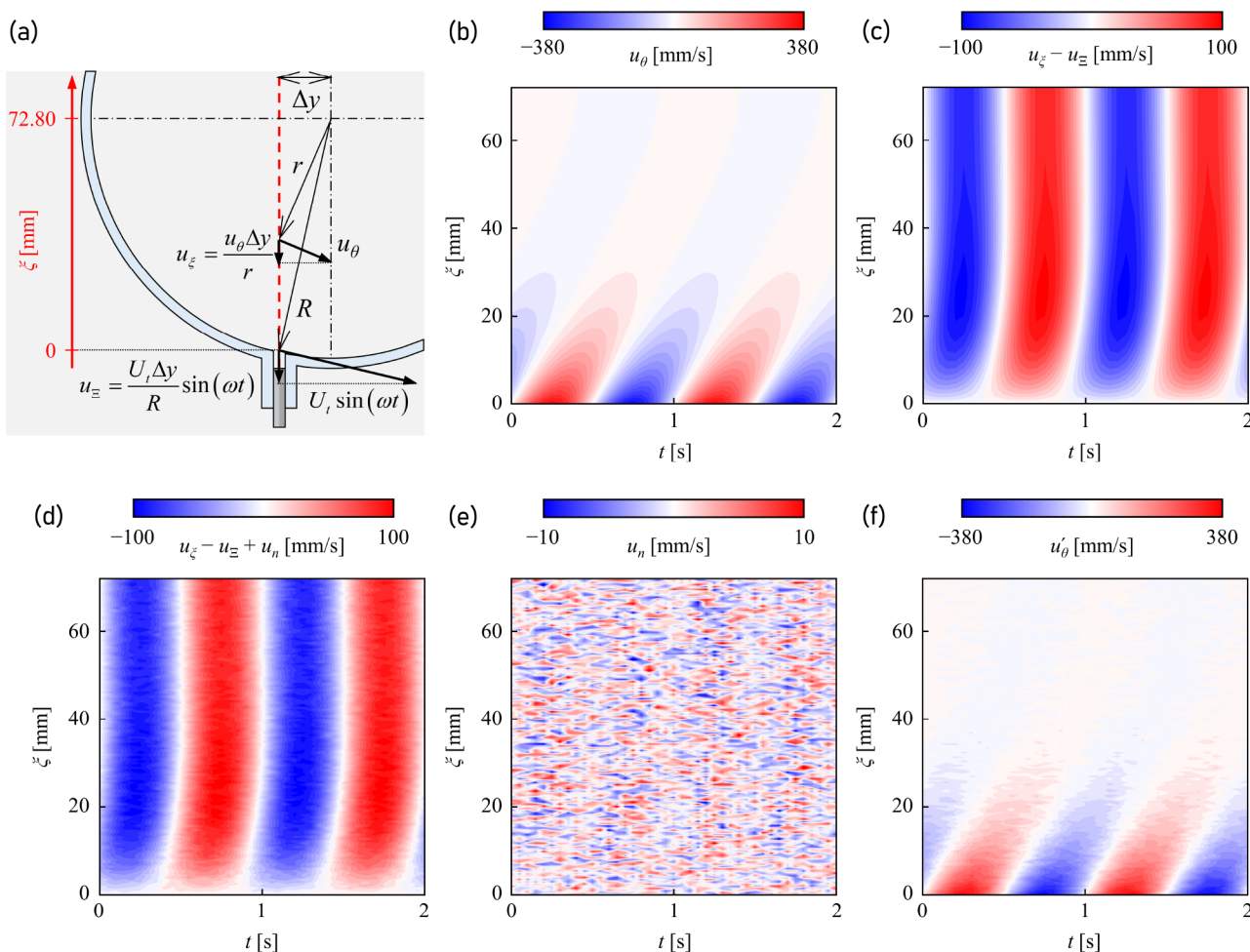


Figure 3. (a) Schematic of geometric condition of exact solution. (b) Spatiotemporal azimuthal velocity distribution (u_θ) at the case of $\mu = 0.3$ Pa·s. (c) Ideal measured velocity distribution ($u_\xi - u_\xi$) along the direction of ultrasonic transducer. (d) Measured velocity distribution with artificially generated noise ($u_\xi - u_\xi + u_n$). (e) Artificially generated noise distribution (u_n). (f) Azimuthal velocity distribution, which is generated as test data for validating the evaluation algorithm. The important parameters for calculating exact solution are summarized in Table 1.

measurement volume of ultrasonic wave pulse has a wider range of radial position as it gets closer to the center. The formula of eq 7 means the fluid behavior has a linear viscoelasticity. The phase difference is defined as $\tan \delta = E/\omega_0 \mu$, where the phase values around $\pi/2$ rad denote the fluid having a high contribution rate of viscous characteristics and smaller values denote a higher contribution rate of elastic characteristics. The efficacy in the application of this constitutive equation to fluids with various rheological characteristics has been proved in previous studies.³⁰

To solve eqs 6 and 7, an evaluation function is defined

$$F(\mu, \delta; r, t) = \left[\rho \frac{\partial u_\theta}{\partial t} - \frac{\partial \tau}{\partial r} - \frac{2\tau}{r} \right]^2 \quad (9)$$

where this equation must satisfy eq 7 as well. By calculating eq 9 in the frequency domain, the unknown term can be reduced because the flow velocity has the dominant frequency f_0 . Values of μ and δ minimizing F can be considered as the optimal solution satisfying the equation of motion and constitutive equation. In this study, the values of μ and δ are obtained by seeking a local minimal value in $F(\mu, \delta)$ with a random search method.³¹ The details of the evaluation of

rheological properties are referred to in previous studies (see refs 22 and 24).

The applicable ranges of $\dot{\gamma}$ and μ are roughly estimated below considering the aspect of experimental limitations. Regarding the range of $\dot{\gamma}$, the highest range is estimated by the applied oscillating angular velocity, $U_{\text{wall}} = 2\pi f_0 R \Theta$. Here, considering the mechanical limitation to the control stepping motor, the range would be up to $O(10^2 \text{ s}^{-1})$ in this study, and it is less as the test fluid viscosity gets thicker. The lowest range is limited by the measurement ability of velocity profiling method. For instance, considering eq 8, the range is roughly estimated as $O(10^{-1} \text{ s}^{-1})$ when the spatial and velocity resolutions are $O(10^{-1} \text{ mm})$ and $O(10^0 \text{ mm/s})$. However, it cannot be quantitatively determined because $\dot{\gamma}$ is influenced by the measurement noise (calculating $\dot{\gamma}$ needs a derivation of u_θ in the radial direction). Regarding the range of μ , both the thickest and thinnest ranges are roughly estimated by considering the relation of the size of measurement volume, viscous layer thickness, and annulus size. As well-known problem of fluid dynamics, the viscous layer thickness is generally given by $\delta_v \sim \sqrt{2\mu/\rho\omega_0}$, where μ , ρ , and ω_0 represent viscosity, density, and oscillation frequency. Here, the relation $a \ll \delta_v < R$ should be satisfied, where a and R

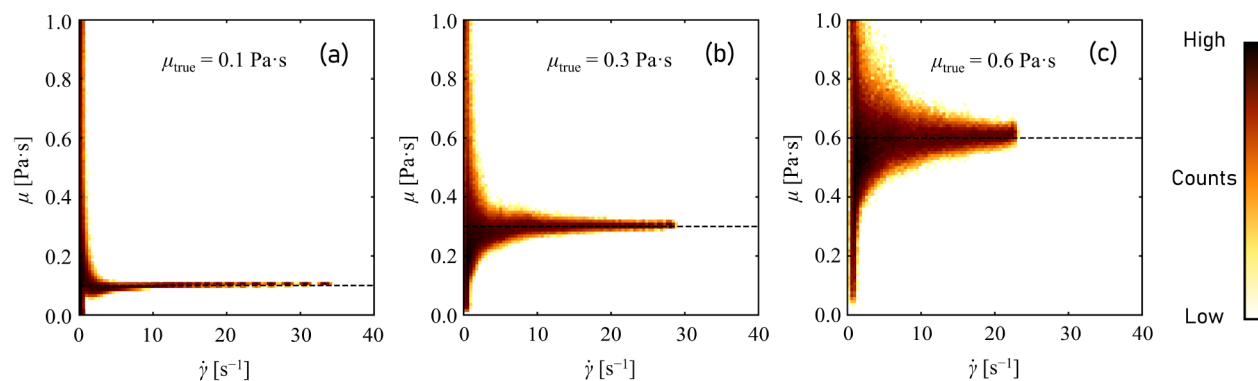


Figure 4. Two-dimensional histograms of $\dot{\gamma}$ and μ , which are obtained by analyzing the artificially generated velocity distribution with different true viscosity μ_{true} : (a) 0.1 Pa·s, (b) 0.3 Pa·s, and (c) 0.6 Pa·s.

Table 1. Summary of Parameters for Calculating Exact Solution

oscillation frequency	f_0	1.0	[Hz]	time resolution	Δt	50	[ms]
oscillation amplitude	Θ	90	[deg]	spatial resolution	$\Delta \xi$	0.49	[mm]
annulus radius	R	75	[mm]	velocity resolution	Δu	1.0	[mm/s]

represent the representative size of the measurement volume, $O(10^{-1} \text{ mm})$, and the radius of the annulus (size of main unit), $O(10^2 \text{ mm})$, so the viscosity range is given by $\rho\omega_0 a^2/2 \ll \mu < \rho\omega_0 R^2/2$, although this would be a rough estimation especially for non-Newtonian fluid ($\mu \neq \text{const.}$). Here, considering the limit of evaluation, it is required that δ_v is at least 10 times as large as a . Therefore, the applicable range of viscosity can be estimated as $O(10^{-2} - 10^0 \text{ Pa}\cdot\text{s})$.

3. NUMERICAL VALIDATION AND EXPERIMENTAL RESULTS

3.1. Efficacy Assessment of Viscosity Evaluation by Artificially Generated Velocity. The efficacy of the measurement method is ensured by analyzing artificially generated velocity data. The generation procedure of the velocity data is explained below. The calculation condition for generating artificial velocity data is described in Figure 3a. First, as shown in Figure 3b, the azimuthal velocity is obtained by the exact solution of the oscillating flow inside the annulus, which is referred to in the appendix in of a previous study.²⁰ Here this velocity is calculated at the spatial position along the dashed line in Figure 3a. In this case, the fluid viscosity and density of the parameter of exact solution are given as 0.3 Pa·s and 1000 kg/m³. The horizontal and vertical axes indicate the time and spatial position ξ . The color contour indicates the amplitude of azimuthal velocity. By adding the transducer velocity u_{Ξ} to the azimuthal velocity u_{θ} , the ideal measured velocity of this geometric condition based on an exact solution can be generated.

In the actual velocity measurement by means of UVP, noises exist with certain intensity depending on the target flow velocity. Thus, artificial noise with the same characteristic as the actual measurement noise is required for ensuring the efficacy of this method. According to the previous study,³² the noise produced by UVP measurement is assumed by a formula as

$$u_n = n_1(0, \alpha|u_{\xi} - u_{\Xi}|) + n_2(0, \beta) \quad (10)$$

where $n(a, b)$ is defined as a function producing a random value with a Gaussian distribution (a : average, \sqrt{b} : standard

deviation). α and β indicate the noise amplitude and basic level of noise, where $\alpha = 0.04$ and $\beta = 0.003$ in this study. Considering eq 10, the intensity of generated noise increases with increasing $|u_{\xi} - u_{\Xi}|$, so this represents the characteristic of measurement noise with the S/N ratio.

The velocity distribution with artificially generated noise is shown in Figure 3d, and the added noise distribution is shown in Figure 3e. After calculating the noise, the velocity distribution of $u_{\xi} - u_{\Xi} + u_n$ is quantized according to the velocity resolution Δu to model the actual velocity distribution measured by UVP. Finally, the azimuthal velocity distribution calculated by eqs 1–4 is obtained as shown in Figure 3f.

Generating velocity data with artificial noise is achieved the same way as mentioned above; numerical validations with three different viscosities ($\mu = 0.1, 0.3, \text{ and } 0.6 \text{ Pa}\cdot\text{s}$) are examined. The evaluation results of rheological properties are indicated as a two-dimensional histogram of μ and $\dot{\gamma}$, shown in Figure 4. The histogram was obtained by counting 1000 cycles of the oscillation period, and the true value of μ was superimposed as a dashed line in Figure 4. The important parameters for calculating velocity distribution by exact solution are summarized in Table 1.

In the case of $\mu = 0.1 \text{ Pa}\cdot\text{s}$, the two-dimensional histogram is shown in Figure 4a. The region with a large number of counts in the histogram distribution has good accordance with the dashed line indicating the set viscosity, except a range of low $\dot{\gamma}$. As shown in Figure 4b,c, the regions with large number of counts has good accordance with the value set as the same as the result in Figure 4a, but the variation in those regions gets larger with increasing μ in the parameter of the exact solution. This error can be lessened by setting a shorter time resolution because the factor of error is considered to increase with the speed of momentum propagation. From these numerical assessments, it is clarified that quality improvements of the evaluation are strongly limited by the measurement performance of velocity profiling.

3.2. Results of Application to Silicon Oil. Silicon oil (Shin-Etsu Chemical Co., Ltd.), with a kinematic viscosity of 300 mm²/s at 25 °C, was selected as a representative example of a Newtonian fluid for ensuring the efficacy of this method.

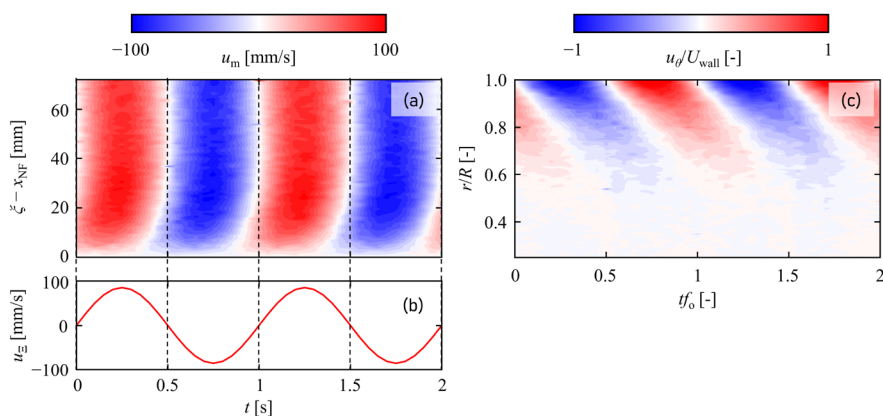


Figure 5. (a) Spatiotemporal measured velocity distribution u_m of silicon oil with the kinematic viscosity $300 \text{ mm}^2/\text{s}$ ($0.29 \text{ Pa}\cdot\text{s}$). (b) Speed of transducer motion in the measured velocity component. (c) Normalized azimuthal velocity distribution, where the oscillation frequency, amplitude, and fluid temperature were 1 Hz , 22.5° , and 25°C , respectively.

The oil has a fluid density of $970 \text{ kg}/\text{m}^3$ and a speed of sound of $980 \text{ m}/\text{s}$. The reserve tank was filled up to the height described in Figure 1a. Since the silicon oil has a kinematic viscosity thinner than $1000 \text{ mm}^2/\text{s}$, it generally shows a pure constant viscosity. To measure the flow velocity by means of UVP, tracer particles (CL-2507; Sumitomo Seika Chemicals Co., Ltd.) were dispersed in the fluid media. Particles are $180 \mu\text{m}$ in mean diameter and $920 \text{ kg}/\text{m}^3$ in density. The particles must have a neutrally buoyancy in the dispersed media or a satisfactory Stokes number $St \ll 1$, where St is a dimensionless number representing the traceability for fluid flows. The volume fraction of dispersed particles is less than 0.1% , so the effects on fluid behavior arising from the particles are negligible. For a better quality of ultrasound echo signal, the measurement parameters in the UVP apparatus were referred to technical note, which was edited by Takeda.³³

With the oscillation frequency $f_0 = 1 \text{ Hz}$ and amplitude $\Theta = 22.5^\circ$, the velocity distribution was measured as shown in Figure 5a, where $U_{\text{wall}} = 185 \text{ mm}/\text{s}$. The horizontal and vertical axes indicate the elapsed time and distance from inner wall along the measurement line. The color contour shows the amplitude of measured velocity u_m . UVP measurement and annulus oscillation were synchronously started, where the moving speed of the transducer u_z is shown in Figure 5b. Comparing the phase of u_m with that of u_z , the phase difference gets larger as it gets closer to the wall ($\xi = 0 \text{ mm}$). Because the phase difference indicates the relative velocity between annulus oscillation and fluid flow inside the annulus, the fluid flow velocity can be extracted by subtracting u_z from u_m , as mentioned in section 3.1.

As shown in Figure 5c, the distribution of azimuthal velocity u_θ is calculated by eq 2. The vertical axis indicates the radial position normalized by the radius of inner annulus, where its unity means the boundary of wall. The horizontal axis indicates the elapsed time normalized by the oscillation frequency, where its integer value means 0 rad in the phase of annulus oscillation. The velocity distribution u_θ has a phase difference showing fluid flows, and this seems to be the same trend with the velocity distribution shown in Figure 3f. In the numerical validation in section 3.1, we did not consider the experimental condition that the measurement volume of ultrasonic wave pulse has a wider range of radial position with getting closer to the annulus center.

Substituting the azimuthal velocity data into eq 9, optimal values of μ and δ are obtained, which minimize the evaluation coefficient F . In addition, the shear strain rate $\dot{\gamma}$ is calculated by substituting the obtained velocity into eq 8. The two-dimensional histogram of $\dot{\gamma}$ and μ is shown in Figure 6. The

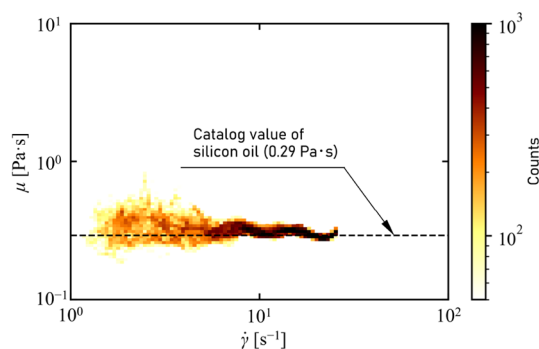


Figure 6. Two-dimensional histograms of $\dot{\gamma}$ and μ , which are obtained by analyzing the velocity distribution of silicon oil with catalog viscosity $0.29 \text{ Pa}\cdot\text{s}$ at 25°C .

horizontal and vertical axes indicate $\dot{\gamma}$ and μ , and the color scale shows count frequency in the histogram, where the total number of oscillation cycles for obtaining the two-dimensional histogram is 200 times.

As seen in Figure 6, showing constant viscosity, the region with high frequency counts has good accordance with the catalog value of silicon oil, regardless of $\dot{\gamma}$. In addition, the deviation of the histogram has $\dot{\gamma}$ dependence following the same trend as the histograms in Figure 4, which were the results evaluating the exact solution with artificial noise. Thus, as a novel *in situ* measurement tool, its efficacy to evaluate the fluid with Newtonian viscosity is ensured through this experiment. As a further improvement for this method, focusing on the histogram in the range of low $\dot{\gamma}$, some factors causing large deviation of frequency counts are considered: (1) the measurement volume having wider range of radial position and (2) the dominance of base noise in the velocity against the azimuthal velocity component. Factor (1) would be solved by improving the surface shape or diameter of the transducer to reduce the expanse of the measurement volume. In this case, ultrasonic waves with stronger amplitude are required for measuring better quality of echo signals from the less tracer

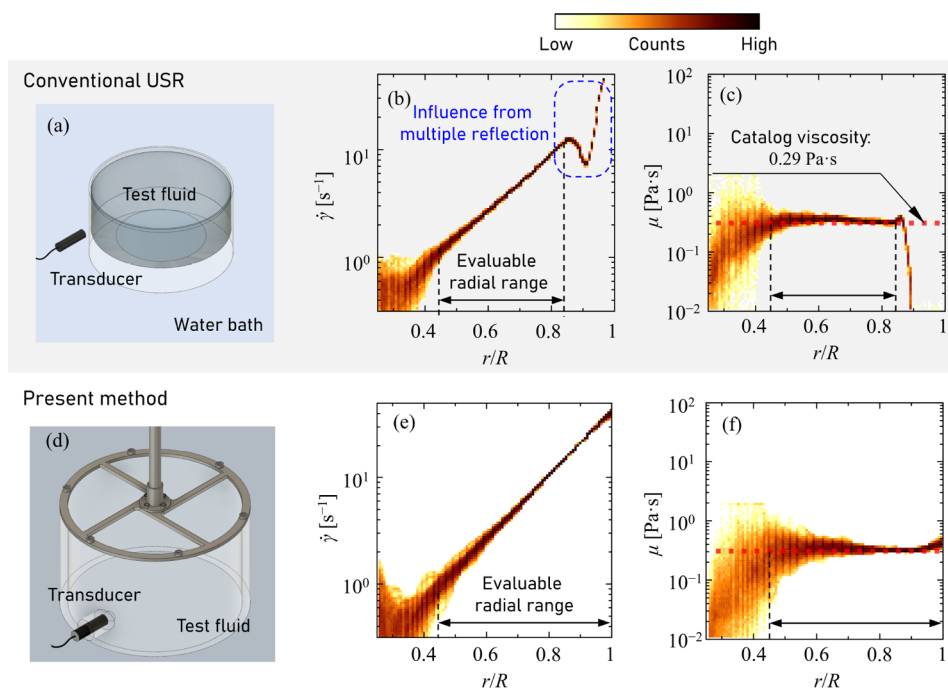


Figure 7. (a) Schematic of conventional USR, and two-dimensional histograms. (b) Relations of r/R and $\dot{\gamma}$. (c) Relation of r/R and μ . (d) Schematic of method proposed in this study, and two-dimensional histograms. (e) Relation of r/R and $\dot{\gamma}$. (f) Relation of r/R and μ , where these results are obtained by analyzing the velocity distribution of silicon oil with catalog viscosity 0.29 Pa·s at 25 °C.

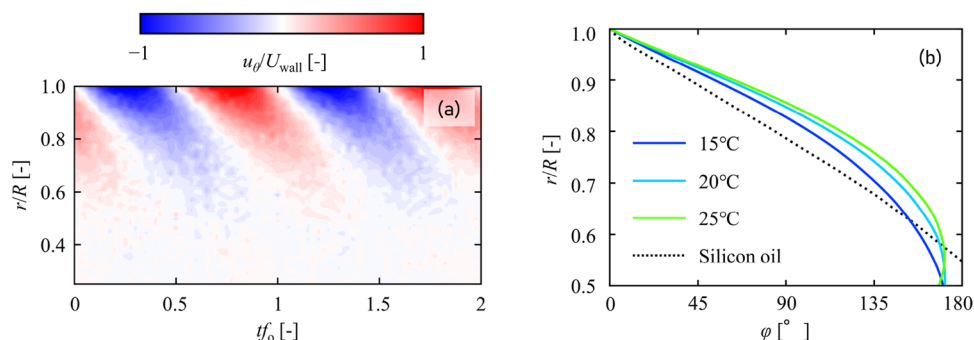


Figure 8. (a) Normalized azimuthal velocity distribution of CMC solution (0.5 wt % and 20 °C). (b) Radial profiles of phase difference φ at each fluid temperature (15, 20, and 25 °C), where the oscillation frequency and amplitude were 0.5 Hz and 90°, respectively.

particles. Factor (2) would be solved by complementary uses of another transducer fixed outside the main unit of oscillating annulus, and because the velocity component of moving transducer in the u_m is zero, the quality of the measured velocity is expected to be better.

In the original configuration of USR (Figure 7a), which evaluates rheological properties by taking samples into a top-open cylindrical container, UVP measurement with an ultrasonic transducer set outside of the container is strongly influenced by multiple reflection of ultrasound at the cylinder wall. The parameters $\dot{\gamma}$ and μ evaluated by conventional USR shown in Figures 7b,c represent odd features of the region near the wall ($r/R = 1$). An embedded transducer in the cylinder wall (Figure 7d), which is one of the modifications from the conventional method, improves the problem caused by multiple reflection. Comparable results obtained by the present method to the conventional USR are shown in Figure 7e,f. Thanks to the improvement, the applicable range of the present method is extended to the immediate vicinity of the wall. The importance of evaluation of rheological properties is

more crucial with getting closer to the wall, because the shear rate amplitude is larger as the location gets closer to the wall, in the case of measuring fluids with shear-rate-dependent properties, such as polymer solutions. The embedded transducer in the present method is also applicable to the conventional USR to improve the applicable range.

3.3. Application to Non-Newtonian Fluid with Shear Thinning Viscosity. Two experiments for carboxymethylcellulose (CMC, provided by Daicel Miraizu, Ltd.) solutions are carried out to show the applicability of our *in situ* measurement tool for fluids with shear thinning viscosity: One is rheological property evaluation of the CMC solution at different set temperatures after a long time has elapsed for reaching equilibrium state of fluid temperature in the tank; the other is rheological property evaluation of the CMC solution under the transient state of fluid temperature changing from 10 to 30 °C. CMC with an etherification degree of 0.63 in was dissolved in tap water to a CMC concentration of 0.5 wt %. Generally, the CMC solution is known as a representative example of fluid with shear thinning viscosity. CHP20/P120 (Mitsubishi

Chemical Co., Ltd.) was used as tracer particle to measure the velocity profiles of CMC solution, and the particle was 75–150 μm in diameter and 1.01 g/mL at 25 $^{\circ}\text{C}$. Using the same UVP measurement approach as in section 3.2, the parameters of UVP were optimized following the instruction described in ref 33. To evaluate the rheological properties at different temperatures, the temperature was maintained by a thermostat for steadily reaching the desired fluid temperature. The speed of sound in the CMC solution is regarded to be the same as that in water (1465.9 m/s at 15 $^{\circ}\text{C}$, 1482.4 m/s at 20 $^{\circ}\text{C}$, and 1496.7 m/s at 25 $^{\circ}\text{C}$, according to ref 34), because the dissolved concentration is so dilute as to not change its speed of sound.

The azimuthal velocity distribution u_{θ} is shown in Figure 8a, where the oscillation frequency f_0 and the amplitude Θ were set at 0.5 Hz and 90 $^{\circ}$, respectively. Given the same azimuthal velocity distribution as that in Figure 5c, the velocity amplitudes are periodically changed with phase difference of momentum propagation due to fluid flow. As shown in Figure 8b, the phase differences φ in the velocity distribution of CMC solutions with different fluid temperatures were quantified as

$$\varphi = \left(\tan^{-1} \frac{\Im[\hat{u}_{\theta}]}{\Re[\hat{u}_{\theta}]} \right) \frac{180}{\pi} - \varphi_{\text{wall}} \quad (11)$$

where the symbol “ \wedge ” denotes operation of Fourier transformation and φ_{wall} indicates the phase value of \hat{u}_{θ} at the wall. The plot shapes of φ under each temperature condition are more rounded compared those with φ in the case of silicon oil, which is shown as the dotted line. According to previous studies, the radial gradient of phase difference represents the rheological property of test fluids as effective Newtonian viscosity. Following the theory, the viscosity of the CMC solution at each temperature condition is qualitatively read as having shear strain rate dependence; instead, the viscosity of silicon oil is read as a constant viscosity regardless of the applied $\dot{\gamma}$. The temperature dependence of viscosity appeared to be the result of the phase differences of CMC solution varying with changing the fluid temperature.

Following the evaluation process explained in section 2, the viscosity of the CMC solution is evaluated from the azimuthal velocity distribution. For CMC solutions with different fluid temperatures, quantitative evaluations of the relation between μ and $\dot{\gamma}$ are shown in Figure 9, with different colored plots (white: 15 $^{\circ}\text{C}$, gray: 20 $^{\circ}\text{C}$, and black: 25 $^{\circ}\text{C}$). With increasing the fluid temperature T , μ in the whole range of $\dot{\gamma}$ decreases. In addition, the variations of μ have a monotonous decrease trend with increasing $\dot{\gamma}$ regardless the fluid temperature T , that is, the

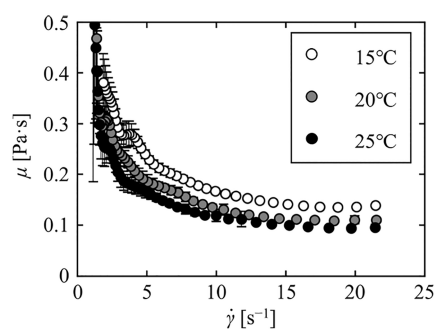


Figure 9. Viscosity evaluation results of CMC solution (0.5 wt %) at each fluid temperature (15, 20, and 25 $^{\circ}\text{C}$).

CMC solution has a typical characteristic of non-Newtonian fluid showing shear thinning viscosity. In addition, the evaluated trends of the viscosity curve of the CMC solution have results qualitatively similar to those reported in previous studies.^{35,36} Thus, the presented method has sufficient efficacy for not only Newtonian fluid but also fluids with shear thinning viscosity.

For ensuring the further applicability of the measurement method, another experiment was conducted below under the condition of continuously increasing fluid temperature. Using the same experimental setup shown in Figure 1, the viscosity of the CMC solution was evaluated simultaneously with temperature (T_{top} and T_{bottom}) measurements at the top and bottom of the tank. This ensures whether a temperature gradient exists in the fluid in tank. After cooling the whole tank to 12 $^{\circ}\text{C}$, it was then heated to 30 $^{\circ}\text{C}$, using a thermostat. Temperature data was obtained as an average value of data with 50 ms temporal resolution and outputted once every second. While the temperature of the test fluid was heated from 12 to 30 $^{\circ}\text{C}$, the velocity of fluid flow and temperature were measured for 10 000 s. With increasing fluid temperature, the speed of sound c gets faster according to Bilaniuk and Wong,³⁴ where fluid temperature is given as $T = (T_{\text{top}} + T_{\text{bottom}})/2$. In this experiment, the speed of sound was also regarded as the same as that of water, as mentioned above. Considering that the characteristic of the speed of sound depends on the fluid temperature, the post processing for correcting spatial position ξ and velocity amplitude u_{ξ} in UVP measurement was carried out as

$$\xi' = c_0 \frac{\lambda c(T)}{2 c_0} \quad (12)$$

$$u_{\xi}' = c_0 \frac{f_D c(T)}{2 f_0 c_0} \quad (13)$$

where $c(T)$, c_0 , λ , f_D , and f_0 denote the speed of sound as a function of fluid temperature,³⁴ speed of sound given as original parameter, time delay between the start of pulse emission and its reception, Doppler shift frequency, and resonance frequency of ultrasound (see ref 33 for details), respectively. The viscosity was intermittently evaluated every 10 s period (20 times of oscillation at $f_0 = 0.5$ Hz) of velocity distribution.

The resulting viscosity contour $\mu(t, \dot{\gamma})$ is shown in Figure 10a, where the fluid temperature monotonically increases as time elapses, as shown in Figure 10b. As seen in the temperature difference between T_{top} and T_{bottom} , there is a negligible gradient of fluid temperature in the tank. With increasing fluid temperature, the viscosity decreases in the whole range of $\dot{\gamma}$, having the characteristic of shear thinning viscosity the same as the results in Figure 9. When the temperature dependence in non-Newtonian fluid is investigated using our method, properties in wide $\dot{\gamma}$ range can be simultaneously measured. This is crucial because only intermittent evaluations of each spot within $\dot{\gamma}$ are obtained by the rotational torque rheometer that is conventionally used. Though deviations on the evaluated viscosity still exist, this result showing transient rheological properties ensures the novelty of our method as an *in situ* measurement.

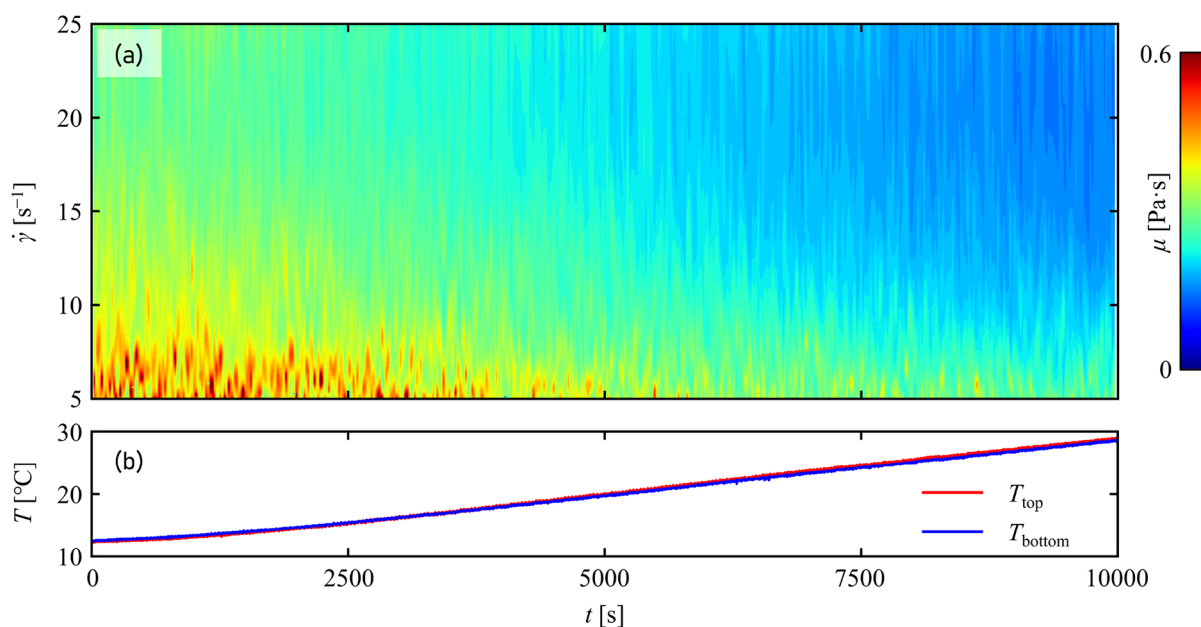


Figure 10. (a) Viscosity contour of CMC solution in elapsed time t and shear strain rate $\dot{\gamma}$ with changing fluid temperature. (b) Time profile of fluid temperature change of CMC solution for 10 000 s.

4. CONCLUSION

In this study, a novel method was presented to develop a tool enabling *in situ* measurement of instantaneous viscosity curve of fluids in a reserve tank, with applicable ranges of shear rate and viscosity, $O(10^{-1}-10^2 \text{ s}^{-1})$ and $O(10^{-2}-10^0 \text{ Pa}\cdot\text{s})$. This method is based on ultrasonic spinning rheometry, which is ideal for practical use owing to its applicability of the ultrasound velocity profiling technique. Through numerical and experimental validations, the efficacy of our method is sufficiently ensured to enable evaluation of rheological properties of Newtonian fluids. Applications to a CMC solution having shear thinning viscosity were also carried out; its shear thinning viscosity was evaluated at stable fluid temperature. As a further challenge in the application to a CMC solution, an important result is the evaluation of the rheological properties of CMC solution in the tank with changing fluid temperature. This achievement implies that this method for the first time realizes evaluations of rheological properties with both dependence of temperature and shear strain rate. To visualize fluid properties in the tank, it should be noted that there is a possibility of further application, such as measurements of viscosity changes during chemical reactions such as gelation, hydrolysis, and polymerization. We conclude that this method is ideally suited for the industrial production process as a novel *in situ* measurement method.

■ AUTHOR INFORMATION

Corresponding Author

Taiki Yoshida – National Institute of Advanced Industrial Science and Technology, 305-8563 Tsukuba, Japan;
 ● orcid.org/0000-0002-9487-6198; Email: taiki.yoshida@aist.go.jp

Authors

Kohei Ohie – Laboratory for Flow Control, Faculty of Engineering, Hokkaido University, Sapporo 060-8628, Japan

Yuji Tasaka – Laboratory for Flow Control, Faculty of Engineering, Hokkaido University, Sapporo 060-8628, Japan; ● orcid.org/0000-0002-8943-4803

Complete contact information is available at:
<https://pubs.acs.org/10.1021/acs.iecr.2c01792>

Author Contributions

T.Y.: Conception and design of study, analysis and interpretation of data, and drafting the manuscript. K.O.: Acquisition of data, interpretation of data, and revising the manuscript. Y.T.: Interpretation of data and revising the manuscript critically for important intellectual content.

Notes

The authors declare no competing financial interest.

■ ACKNOWLEDGMENTS

This work was supported by JSPS, KAKENHI Grant Number 22K14186, and JST, PRESTO Grant Number JPMJPR21O6.

■ REFERENCES

- (1) Broadhead, T.; Patterson, W.; Dealy, J. Closed loop viscosity control of reactive extrusion with an in-line rheometer. *Polym. Eng. Sci.* **1996**, *36*, 2840–2851.
- (2) Covas, J.; Nóbrega, J. M.; Maia, J. M. Rheological measurements along an extruder with an on-line capillary rheometer. *Polym. Test.* **2000**, *19*, 165–176.
- (3) Glasscock, J.; Smith, R.; Vanajek, J.; Winter, J. An in-line micro-Fourier rheometer. *Rev. Sci. Instrum.* **2003**, *74*, 4925–4929.
- (4) Møller, P. C. F.; Mewis, J.; Bonn, D. Yield stress and thixotropy: on the difficulty of measuring yield stresses in practice. *Soft Matter* **2006**, *2*, 274–283.
- (5) Nechyporchuk, O.; Belgacem, M. N.; Pignon, F. Rheological properties of micro-/nanofibrillated cellulose suspensions: Wall-slip and shear banding phenomena. *Carbohydr. Polym.* **2014**, *112*, 432–439.
- (6) Fardin, M. A.; Casanellas, L.; Saint-Michel, B.; Manneville, S.; Lerouge, S. Shear-banding in wormlike micelles: Beware of elastic instabilities. *J. Rheol.* **2016**, *60*, 917–926.

- (7) Guillemain, J.-P.; Ménard, Y.; Brunet, L.; Bonnefoy, O.; Thomas, G. Development of a new mixing rheometer for studying rheological behaviour of concentrated energetic suspensions. *J. Non-Newtonian Fluid Mech.* **2008**, *151*, 136–144.
- (8) Coogan, T. J.; Kazmer, D. O. In-line rheological monitoring of fused deposition modeling. *J. Rheol.* **2019**, *63*, 141–155.
- (9) Wallevik, J. E.; Wallevik, O. H. Concrete mixing truck as a rheometer. *Cem. Concr. Res.* **2020**, *127*, 105930.
- (10) Dimitriou, C. J.; Casanellas, L.; Ober, T. J.; McKinley, G. H. Rheo-PIV of a shear-banding wormlike micellar solution under large amplitude oscillatory shear. *Rheol. Acta* **2012**, *51*, 395–411.
- (11) Martin, J. D.; Hu, Y. T. Transient and steady-state shear banding in aging soft glassy materials. *Soft Matter* **2012**, *8*, 6940–6949.
- (12) Derakhshandeh, B.; Vlassopoulos, D.; Hatzikiriakos, S. G. Thixotropy, yielding and ultrasonic Doppler velocimetry in pulp fibre suspensions. *Rheol. Acta* **2012**, *51*, 201–214.
- (13) Gallot, T.; Perge, C.; Grenard, V.; Fardin, M. A.; Taberlet, N.; Manneville, S. Ultrafast ultrasonic imaging coupled to rheometry: Principle and illustration. *Rev. Sci. Instrum.* **2013**, *84*, 045107.
- (14) Fischer, P.; Wheeler, E. K.; Fuller, G. G. Shear-banding structure orientated in the vorticity direction observed for equimolar micellar solution. *Rheol. Acta* **2002**, *41*, 35–44.
- (15) Divoux, T.; Fardin, M. A.; Manneville, S.; Lerouge, S. Shear banding of complex fluids. *Annu. Rev. Fluid Mech.* **2016**, *48*, 81–103.
- (16) McKinley, G. H.; Byars, J. A.; Brown, R. A.; Armstrong, R. C. Observations on the elastic instability in cone-and-plate and parallel-plate flows of a polyisobutylene Boger fluid. *J. Non-Newtonian Fluid Mech.* **1991**, *40*, 201–229.
- (17) Fardin, M. A.; Perge, C.; Casanellas, L.; Hollis, T.; Taberlet, N.; Ortin, J.; Lerouge, S.; Manneville, S. Flow instabilities in large amplitude oscillatory shear: A cautionary tale. *Rheol. Acta* **2014**, *53*, 885–898.
- (18) Wiklund, J.; Stading, M.; Trägårdh, C. Monitoring liquid displacement of model and industrial fluids in pipes by in-line ultrasonic rheometry. *J. Food Eng.* **2010**, *99*, 330–337.
- (19) Tasaka, Y.; Yoshida, T.; Murai, Y. Nonintrusive in-line rheometry using ultrasonic velocity profiling. *Ind. Eng. Chem. Res.* **2021**, *60*, 11535–11543.
- (20) Tasaka, Y.; Kimura, T.; Murai, Y. Estimating the effective viscosity of bubble suspensions in oscillatory shear flows by means of ultrasonic spinning rheometry. *Exp. Fluids* **2015**, *56*, 1867.
- (21) Yoshida, T.; Tasaka, Y.; Murai, Y. Rheological evaluation of complex fluids using ultrasonic spinning rheometry in an open container. *J. Rheol.* **2017**, *61*, 537–549.
- (22) Tasaka, Y.; Yoshida, T.; Rapberger, R.; Murai, Y. Linear viscoelastic analysis using frequency-domain algorithm on oscillating circular shear flows for bubble suspensions. *Rheol. Acta* **2018**, *57*, 229–240.
- (23) Yoshida, T.; Tasaka, Y.; Tanaka, S.; Park, H. J.; Murai, Y. Rheological properties of montmorillonite dispersions in dilute NaCl concentration investigated by ultrasonic spinning rheometry. *Appl. Clay Sci.* **2018**, *161*, 513–523.
- (24) Yoshida, T.; Tasaka, Y.; Murai, Y. Efficacy assessments in ultrasonic spinning rheometry: Linear viscoelastic analysis on non-Newtonian fluids. *J. Rheol.* **2019**, *63*, 503–517.
- (25) Yoshida, T.; Tasaka, Y.; Fischer, P. Ultrasonic spinning rheometry test on the rheology of gelled food for making better tasting desserts. *Phys. Fluids* **2019**, *31*, 113101.
- (26) Yoshida, T.; Tasaka, Y.; Murai, Y. Effective viscoelasticity of non-Newtonian fluids modulated by large-spherical particles aligned under unsteady shear. *Phys. Fluids* **2019**, *31*, 103304.
- (27) Yoshida, T.; Tasaka, Y.; Fischer, P.; Murai, Y. Time-dependent viscoelastic characteristics of montmorillonite dispersion examined by ultrasonic spinning rheometry. *Appl. Clay Sci.* **2022**, *217*, 106395.
- (28) Ohie, K.; Yoshida, T.; Tasaka, Y.; Murai, Y. Effective rheology mapping for characterizing polymer solutions utilizing ultrasonic spinning rheometry. *Exp. Fluids* **2022**, *63*, 40.
- (29) Ohie, K.; Yoshida, T.; Park, H. J.; Tasaka, Y.; Murai, Y. Evaluation on time variation of effective viscosity by ultrasonic spinning rheometry (Application to separating oil-water mixture). *Trans. Jpn. Soc. Mech. Eng.* **2020**, *86*, 20-0042. (in Japanese).
- (30) Yoshida, T.; Tasaka, Y.; Ohie, K.; Murai, Y. Overview of Ultrasonic Spinning Rheometry: Application to Complex Fluids. *Nihon Reorogi Gakkaishi* **2022**, *50*, 3–7.
- (31) Solis, F. J.; Wets, R. J.-B. Minimization by random search techniques. *Math. Oper. Res.* **1981**, *6*, 19–30.
- (32) Yoshida, T.; Tasaka, Y.; Park, H. J.; Murai, Y. Accuracy and robustness evaluations on algorithms of ultrasonic spinning rheometry. *Proc. 11th Int. Symp. Ultrason. Doppler Methods Fluid Mech. Fluid Eng.* **2018**, 56–59.
- (33) Takeda, Y., Ed. *Ultrasonic Doppler Velocity Profiler for Fluid Flow*; Fluid Mechanics and Its Applications, series Vol. 101; Springer: Japan, 2012.
- (34) Bilaniuk, N.; Wong, G. S. Speed of sound in pure water as a function of temperature. *J. Acoust. Soc. Am.* **1993**, *93*, 1609–1612.
- (35) Ghannam, M. T.; Esmail, M. N. Rheological properties of carboxymethyl cellulose. *J. Appl. Polym. Sci.* **1997**, *64*, 289–301.
- (36) Yang, X. H.; Zhu, W. L. Viscosity properties of sodium carboxymethylcellulose solutions. *Cellulose* **2007**, *14*, 409–417.

Recommended by ACS

New Method for Gelation Temperature Measurement without Disturbing the Crystal Network

Sachin Balasaheb Shinde and Lalit Kumar

JUNE 03, 2021

INDUSTRIAL & ENGINEERING CHEMISTRY RESEARCH

READ 

Experimental High-Temperature, High-Pressure Density Measurement and Perturbed-Chain Statistical Associating Fluid Theory Modeling of Dimethyl Sulf...

Ameneh Paknejad, Hosseinali Zarei, et al.

OCTOBER 15, 2019

JOURNAL OF CHEMICAL & ENGINEERING DATA

READ 

Wertheim Model for Quantum Associating Hard Spheres

Sergio Contreras, Alejandro Gil-Villegas, et al.

NOVEMBER 16, 2020

JOURNAL OF CHEMICAL & ENGINEERING DATA

READ 

Computation of Isobaric Thermal Expansivity from Liquid Density Measurements. Application to Toluene

Jean-Luc Daridon, Jean-Patrick Bazile, et al.

OCTOBER 05, 2021

JOURNAL OF CHEMICAL & ENGINEERING DATA

READ 

Get More Suggestions >